Ships and Offshore Structures

ISSN: (Print) (Online) Journal homepage: https://www.tandfonline.com/loi/tsos20

Numerical modelling of spoolable thermoplastic composite pipe (TCP) under combined bending and thermal load

James C. Hastie, Igor A. Guz & Maria Kashtalyan

To cite this article: James C. Hastie, Igor A. Guz & Maria Kashtalyan (2022) Numerical modelling of spoolable thermoplastic composite pipe (TCP) under combined bending and thermal load, Ships and Offshore Structures, 17:9, 1975-1986, DOI: 10.1080/17445302.2021.1958534

To link to this article: https://doi.org/10.1080/17445302.2021.1958534

SHIPS AND OFFSHORE STRUCTURES
2022, VOL. 17, NO. 9, 1975–1986
https://doi.org/10.1080/17445302.2021.1958534

Taylor & Francis
Taylor & Francis Group

Numerical modelling of spoolable thermoplastic composite pipe (TCP) under combined bending and thermal load

James C. Hastie [a,b], Igor A. Guz [a,b] and Maria Kashtalyan [a,b]

[a]School of Engineering, University of Aberdeen, Scotland, UK; [b]Centre for Micro- and Nanomechanics (CEMINACS), UK

ABSTRACT

Spoolable thermoplastic composite pipe (TCP) consisting of fibre-reinforced laminate with inner and outer liners is an ideal candidate to replace steel counterparts in deepwater. In this paper, a 3D finite element (FE) model is developed to analyse stresses in TCP under combined bending and uniform temperature change illustrative of spooling in different environments. Thermal load causes deviation from the stress symmetry expected at the top/bottom of the pipe in simple bending. Maximum stress, Tsai–Hill and Hashin failure responses are analysed for $[\pm 55]_4$, $[\pm 42.5]_4$, $[\pm 30]_4$ and $[(\pm 55)_2/(\pm 30)_2]$ laminates at low and high temperatures. The $[\pm 42.5]_4$ configuration displays superior spooling capacity as layers orientated at ±55° and ±30° exhibit high utilisation of relatively weak transverse tensile and fibre compressive strengths, respectively. The failure criteria are in closest agreement at the top of the pipe (under axial tension) but differ more significantly at the bottom (axial compression).

ARTICLE HISTORY
Received 17 May 2021
Accepted 1 July 2021

KEYWORDS
Thermoplastic composite pipe; pipe bending; finite element modelling; thermomechanical analysis; composite failure criteria

Nomenclature

E	Elastic modulus (isotropic)
E_1, E_2, E_3	Elastic moduli in material coordinates
f^{H}, f^{MS}, f^{TH}, f^{VM}	Hashin, Maximum stress, Tsai–Hill, von Mises failure coefficients
f^{H1}, f^{H2}, f^{H3}, f^{H4}	Hashin mode coefficients
G_{23}, G_{13}, G_{12}	Shear moduli in material coordinates
K	Curvature
k	Layer number
L	Section length
M	Bending moment
m, n	Cosine of fibre angle, sine of fibre angle
N	Number of layers
Q, R, S	Shear strengths in material coordinates (23, 13, 12)
R	Bending radius
r	Radius
r_0, r_a	Inner radius, outer radius
T	Temperature
ur_X, ur_Y, ur_Z	Rotations about global axes
u_X, u_Y, u_Z	Displacements in global coordinates
X_C, Y_C, Z_C	Compressive strengths in material coordinates (1, 2, 3)
X_T, Y_T, Z_T	Tensile strengths in material coordinates (1, 2, 3)
α	Thermal expansion coefficient (isotropic)
α_1, α_2, α_3	Thermal expansion coefficients in material coordinates
θ	Rotation about longitudinal axis
λ	Thermal conductivity (isotropic)
λ_1, λ_2, λ_3	Thermal conductivities in material coordinates
ν	Poisson's ratio (isotropic)
ν_{23}, ν_{13}, ν_{12}	Poisson's ratios in material coordinates
σ_1, σ_2, σ_3	Normal stresses in material coordinates
σ_y	Yield strength (isotropic)
σ_z, σ_θ, σ_r	Normal stresses in cylindrical coordinates
τ_{23}, τ_{13}, τ_{12}	Shear stresses in material coordinates
$\tau_{\theta r}$, τ_{zr}, $\tau_{z\theta}$	Shear stresses in cylindrical coordinates
φ	Fibre angle

1. Introduction

Compared to traditional steels, fibre-reinforced plastic (FRP) materials offer a number of advantages for offshore exploration and production (E&P) applications, including reduced weight, superior fatigue performance and corrosion resistance. The uptake of composite materials in the industry was historically hindered by the lack of performance track records, regulatory requirements and efficient design procedures (Guz et al. 2017). However, in recent years, the spotlight has shifted to composites and particularly FRPs as enabling technologies for exploiting deeper waters and harsher environments. Thermoplastic composite pipe (TCP) is a spoolable pipe solution gaining prominence, driven by the advent of its own design standard (DNV GL 2018).

TCP is operating in downline and jumper applications worldwide and is attracting interest for ultra deepwater riser systems (Smits et al. 2018). TCP consists of an inner thermoplastic liner, fibre-reinforced thermoplastic laminate and outer thermoplastic liner (coating). The composite laminate, comprising unidirectional layers stacked in engineered orientations, is formed by automated winding and serves as the primary load carrier. Thick layers can be produced by continually winding at the same fibre angle. The liners are extruded and provide fluid-tightness and protection from the environment. Thermoplastics including polyethylene (PE), polyamide (PA), polyvinylidene fluoride (PVDF) and polyetheretherketone (PEEK) can be used, preferred over thermosets for ductility, fracture toughness, impact resistance and the ability to consolidate in a single step. The laminate is typically reinforced with carbon or glass fibres. A melt-fusion process typified by leading manufacturers is used to bond the thermoplastic throughout the wall, which prevents non-bonded pipe problems such as rapid gas decompression (van Onna et al. 2012). During subsea operation, TCP is subjected to combinations of mechanical loads and thermal gradients arising from the mismatch between internal and external temperatures. The pipe is subjected to large bending moments when spooled for storage and installation.

The behaviour of FRP tubulars under pure bending has been well studied. Xia et al. (2002) presented an exact solution based on classical laminated-plate theory for sandwich pipes with filament-wound skins. They showed that stresses and strains

CONTACT James C. Hastie r03jh15@abdn.ac.uk

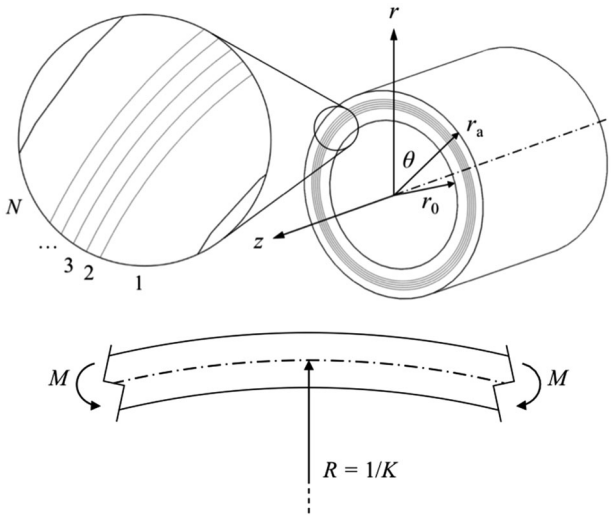

Figure 1. TCP under bending.

depend strongly on winding angle. Natsuki et al. (2003) adopted laminated-plate theory to study bending of filament-wound pipes. Maximum stress failure predictions agreed closely with four-point test results. The theoretical framework was used by Menshykova and Guz (2014) to compare stresses in carbon/epoxy pipes with inner steel or 0° fibre layers and by Cox et al. (2019), who assessed spooling of different pipe geometries and layups. Shadmehri et al. (2011) closely predicted experimental bending stiffness of carbon/polyetherketoneketone (PEKK) tubes by non-classical beam theory accounting for shear deformation. They found the moment of inertia approach closely predicted stiffness of cross-ply tubes only. Geuchy Ahmad and Hoa (2016) later showed agreement between bending stiffness of thick carbon/PEEK tubes determined experimentally and calculated using the 3D elasticity formula derived by Jolicoeur and Cardou (1994). Tubes comprising a high number of alternating ±25° layers were marginally stiffer than tubes with only two thick layers. Ashraf et al. (2014) studied nonlinear bending of carbon/PEEK TCP with different thickness-to-diameter ratios and fibre orientations by finite element (FE) shell modelling. Increasing axial strength by orienting plies at a low angle comes at the expense of larger spooling radii. Huang et al. (2020) developed a continuum shell model for progressive failure analysis (PFA) of carbon/epoxy pipes under bending. Damage was evaluated according to the Hashin criterion with an energy-based linear softening rule to describe damage evolution. Moshir et al. (2020) accurately determined strains in thick carbon/PEEK tubes under bending by 3D finite element analysis (FEA).

'Reinforced thermoplastic pipe (RTP)' is a term for pipe resembling the TCP arrangement consisting of layers of unidirectional tape-wound aramid/high-density polyethylene (HDPE) with HDPE liners. Bai et al. (2015a) developed a simplified model for ovalisation instability of RTP under bending based on the metallic pipe theory of Kyriakides and Ju (1992) and Ju and Kyriakides (1992). Composite layers were modelled as HDPE with a reduction factor for omitted fibres. Yu et al. (2015) studied the flexural behaviour of RTP with different diameter-to-thickness ratios and ply angles by FEA. They accounted for strain-dependent behaviour and geometric nonlinearity in their shell model. Cao et al. (2017) investigated the bending of RTP during pipe-lay installation by numerical simulations incorporating validated nonlinear vessel motions. RTP behaviour under bending combined with external pressure (Bai et al. 2015b) or tension (Bai et al. 2014) has been investigated.

Table 1. TCP dimensions.

Dimension	Value
Inner radius, r_0 (mm)	76
Inner liner thickness (mm)	8
Composite laminate thickness (mm)	8
Outer liner thickness (mm)	8
Outer radius, r_a (mm)	100

The E&P sector continues to expand globally and TCP may be deployed in cold or hot climates. It is therefore important to investigate how TCP responds when spooled at different temperatures. Tubulars consisting of multiple isotropic layers, orthotropic layers or a combination have been studied under thermomechanical loading. In general, the literature mostly covers analytical or semi-analytical modelling of tubulars subjected to pressure combined with uniform temperature change (Xia et al. 2001; Akçay and Kaynak 2005) or through-wall thermal gradient (Bakaiyan et al. 2009; Zhang et al. 2012). FEA has not been extensively employed. Yousefpour and Nejhad (2004) performed a nonlinear FEA of a carbon/PEEK vessel under external pressure and hygrothermal loading. Varying the temperature 0–60°C (from initial 23°C) with 0.23% absorption by weight had a negligible effect on strength or buckling. Rodriguez and Ochoa (2004) developed an FE shell model accounting for geometric nonlinearity and thermal residual stresses to simulate four-point bending tests of filament-wound tubes. Their model incorporated a progressive damage subroutine based on Maximum Stress, Hashin or Hashin–Rotem failure criteria. Almeida et al. (2014) investigated carbon/epoxy pipes with winding angles ranging from ±35° to ±75° under pressure considering hygrothermal conditioning by 3D FEA. Predicted burst pressure decreased by 2–3% based on coefficients obtained from 30-day submersions of specimens at 80°C. Hastie et al. (2019a, 2019b, 2020) performed 3D FEA to investigate the influence of thermal gradient on the failure of carbon/PEEK TCP under combined pressures and tensions illustrative of deepwater riser operation. The effects of increasing operating temperature are less pronounced under high pressure where the laminate experiences greater utilisation. A similar study demonstrated the effects of varying temperature profiles on pressurised sandwich pipe with carbon/PEEK skins and PEEK core depend on whether loading is hoop-dominated or biaxial (Hastie et al. 2021).

TCP is subjected to various operational, environmental and potentially accidental loads during its lifetime. Dedicated FE software packages afford the ability to introduce a variety of loads to established models. For example, one could study spooling of TCP and subsequently operating loads (pressure, tension) or accident scenarios (lateral impacts). Furthermore, imperfections can be incorporated, whereas this may prove analytically unfeasible. In this paper, a 3D FE model is developed to analyse stresses in TCP under combined bending and uniform temperature change illustrative of spooling in different environments (the effects of large, rapid temperature fluctuations associated with operation are left for a future study). To the authors' best knowledge, the response of TCP under such combination has not previously been studied. The nearest existing work appears to be the shell modelling of filament-wound tubes performed by Rodriguez and Ochoa (2004), who added residual stresses to corresponding components in the first increment of incremental bending. Here, we analyse static bending and thermal load applied simultaneously accounting for temperature-dependent 3D properties. Carbon/PEEK is attractive for deepwater applications and was selected to extend the aforementioned carbon/PEEK research. Elastic moduli under compression are assumed to be equal to the tensile moduli

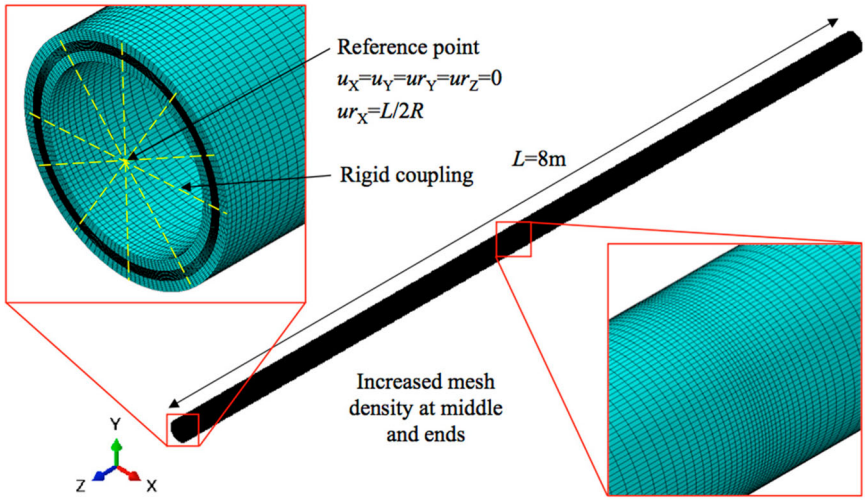

Figure 2. TCP model, global coordinates and constraints (symmetric at both ends). (This figure is available in colour online.)

considering simple bending in line with the above-reviewed literature, including recent works on carbon/PEEK (Ashraf et al. 2014; Geuchy Ahmad and Hoa 2016; Moshir et al. 2020), i.e. known differences in moduli (around 10%) are deemed negligible. Failure predictions based on the limit, interactive and mode-based criteria are compared for different laminate configurations under bending at reduced and elevated temperatures and the implications of fibre angle optimisation on practical spooling radii are evaluated.

2. Methodology

2.1. Finite element model

Let us consider a section of TCP with N total layers in cylindrical coordinates under bending moment, M, as illustrated in Figure 1. Layers $k = 1$ and $k = N$ are isotropic liners and the remaining are orthotropic layers that constitute the composite laminate. A 3D section of TCP with dimensions in Table 1 was modelled in Abaqus/CAE 2019. The laminate is composed of eight 1 mm thick unidirectional layers. Perfect bonding is assumed. In this paper, we investigate the response of different laminations that will be later described. The TCP resembles a real-world configuration but is not intended to emulate any one product exactly.

The model, global coordinates and constraints are shown in Figure 2. A single part is partitioned into layers with discrete orientations. Bending is imposed via rotation ur_X applied to reference points located at the centre of each end. Boundary conditions are defined at the points to keep end sections circular and allow axial displacement, i.e. $u_X = u_Y = ur_Y = ur_Z = 0$. All available degrees of freedom at the end face nodes are constrained to the corresponding points via kinematic couplings. The total angle of rotation in radians is L/R, where $L = 8$ m is the length of the section ($L/r_a = 80$) and R is the bending radius ($R = 1/K$; K is the curvature). Results are measured through the middle of the pipe.

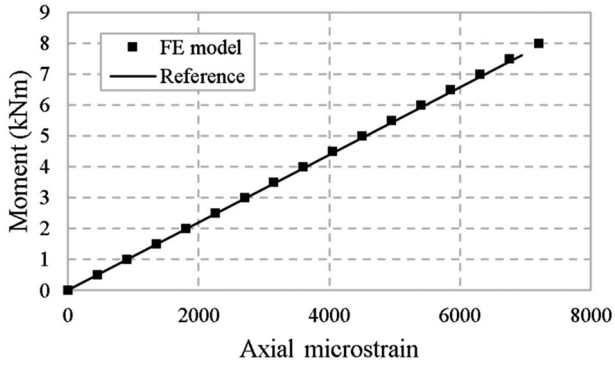

Figure 3. Comparison between validation model and theoretical moment vs. axial strain for carbon/PEEK [±25] pipe presented by Geuchy Ahmad and Hoa (2016).

Moshir et al. (2020) demonstrated that 3D FEA can accurately predict experimental bending strains in thick carbon/PEEK tubes. They simulated four-point bending instigated via vertical loads and supports. To validate the present constraints, a model of the thick carbon/PEEK tube with [±25] stacking sequence studied by Geuchy Ahmad and Hoa (2016) was created. In the previous work, they calculated stiffness using 3D elasticity theory, which yields more accurate solutions than classical or shear deformation theories for thick laminates that exhibit cross-sectional warping and zigzagged distribution of through-thickness in-plane displacement. A comparison of moment vs. axial strain plots computed using the FE model and calculated by Geuchy Ahmad and Hoa (2016) is shown in Figure 3. Close agreement between methods demonstrates the suitability of the FE modelling approach for a thick carbon/PEEK pipe with linear elastic response. The model was meshed using quadratic reduced-integration elements C3D20R that do not experience the hour-glassing phenomenon that affects linear elements.

In the bending–thermal TCP model, the loads are applied simultaneously in a coupled temperature-displacement step. Temperature is applied as a boundary condition. Element type C3D20RT was used (thermal version of C3D20R). Appropriate mesh density and model length were determined by convergence. Temperature-dependent properties of unidirectional AS4/APC-2 and neat APC-2 used to define the materials are presented in Tables 2 and 3. APC-2 has a glass transition temperature of 143°C and can be used up to 260°C due to its semi-crystalline nature (Cytec 2012).

A comprehensive source for temperature-dependent properties of unidirectional carbon/PEEK is not readily available. Temperature-dependency has often been overlooked in composite analyses, one infers due to the difficulty in sourcing properties or practical/cost limitations associated with experiments (which were outwith this work scope). Properties here were compiled from the literature (Coquill and Adams 1989; Cytec 2012; Grove 1988; Jones et al.

Table 2. Properties of AS4/APC-2 carbon/PEEK.

Property	0°C	50°C
E_1 (GPa)	145.29	138.15
$E_2 = E_3$ (GPa)	9.90	9.25
G_{23} (GPa)	3.73	3.47
$G_{13} = G_{12}$ (GPa)	6.36	5.58
ν_{23}	0.328	0.332
$\nu_{13} = \nu_{12}$	0.368	0.373
α_1 (°C^{-1})	$-0.18 \times 10-^{6}$	-0.18×10^{-6}
$\alpha_2 = \alpha_3$ (°C^{-1})	23.94×10^{-6}	23.94×10^{-6}
λ_1 (W m^{-1} °C^{-1})	3.82	4.22
$\lambda_2 = \lambda_3$ (W m^{-1} °C^{-1})	0.40	0.45
X_T (MPa)	2088.50	2048.24
$Y_T = Z_T$ (MPa)	82.88	74.44
X_C (MPa)	1257.70	1134.34
$Y_C = Z_C$ (MPa)	187.17	166.58
Q (MPa)	96.48	86.09
$R = S$ (MPa)	195.09	174.02

1985; Ramey and Palazotto 1989; Rule and Sparks 1990; Sun and Rui 1989; Yousefpour and Nejhad 2004). To the authors' best knowledge, this list represents the most complete compilation of properties for the temperature range. The following assumptions were made to fully define the materials. For the real-world design, the properties should be actively determined experimentally and the configuration here represents achievable performance only.

- Available data are linearly inter/extrapolated over the temperature range.
- E_1, E_2 and E_3 are tensile moduli and assumed to be the same under compression, which is typical in FRP modelling (e.g. works surveyed earlier) and follows simple bending theory. In reality, FRP compressive moduli are around 10% lower than the tensile (Meng et al. 2015) and scarcely quantified at temperature. Switching moduli in the constitutive equations for negative strain directions would increase complexity with relatively little practical gain. We note that legislating for differences becomes important when studying phenomena linked with pure compression.
- Thermal expansion coefficients for carbon/PEEK and PEEK at room temperature (23°C) reported by Yousefpour and Nejhad (2004) and Coquill and Adams (1989) are assumed to remain constant with temperature.
- Shear modulus G_{23} is calculated as

$$G_{23} = \frac{E_2}{2(1+\upsilon_{23})} \tag{1}$$

- Poisson's ratio ν_{23} at room temperature (Yousefpour and Nejhad 2004) is assumed to vary with temperature at the rate reported for ν_{13} and ν_{12} (Ramey and Palazotto 1989).
- Shear strength Q at room temperature (Yousefpour and Nejhad 2004) is assumed to vary with temperature at the rate reported for R and S (Cytec 2012).

Table 3. Properties of APC-2 PEEK.

Property	0°C	50°C
E (GPa)	4.25	3.95
N	0.406	0.421
α (°C^{-1})	50.80×10^{-6}	50.80×10^{-6}
λ (W m^{-1} °C^{-1})	0.27	0.29
σ_y (MPa)	117.58	85.22

2.2. Failure criteria

Stresses obtained by FEA are used to evaluate liner yielding according to von Mises criterion and failure of FRP layers according to limit, interactive and failure mode-based criteria. These are the Maximum stress (herein 'Max Stress'), Tsai–Hill and Hashin criteria, respectively. We consider first-ply failure (FPF) as opposed to progressive failure on the basis that an undamaged pipe is desired beyond spooling.

The von Mises coefficient is expressed as

$$f^{\mathrm{VM}} = \sqrt{\frac{(\sigma_1-\sigma_2)^2+(\sigma_2-\sigma_3)^2+(\sigma_3-\sigma_1)^2}{2}}\frac{1}{\sigma_y}, \tag{2}$$

where σ_y is the yield strength (failure occurs when $f^{\mathrm{VM}} = 1.0$).

Stresses in principal material coordinates are used to assess the failure of orthotropic layers, related to cylindrical coordinates by

$$\begin{Bmatrix}\sigma_1\\ \sigma_2\\ \sigma_3\\ \tau_{23}\\ \tau_{13}\\ \tau_{12}\end{Bmatrix} = \begin{bmatrix} m^2 & n^2 & 0 & 0 & 0 & 2mn \\ n^2 & m^2 & 0 & 0 & 0 & -2mn \\ 0 & 0 & 1 & 0 & 0 & 0 \\ 0 & 0 & 0 & m & -n & 0 \\ 0 & 0 & 0 & n & m & 0 \\ -mn & mn & 0 & 0 & 0 & m^2-n^2 \end{bmatrix} \begin{Bmatrix}\sigma_z\\ \sigma_\theta\\ \sigma_r\\ \tau_{\theta r}\\ \tau_{zr}\\ \tau_{z\theta}\end{Bmatrix}, \tag{3}$$

where $m = \cos\varphi$ and $n = \sin\varphi$; φ is the fibre angle with respect to the pipe longitudinal axis. According to Max Stress, failure occurs when any principal stress exceeds the corresponding allowable. The coefficient is

$$f^{\mathrm{MS}} = \max\left\{\frac{\sigma_1}{X_T}\text{ or }\frac{|\sigma_1|}{X_C}, \frac{\sigma_2}{Y_T}\text{ or }\frac{|\sigma_2|}{Y_C}, \frac{\sigma_3}{Z_T}\text{ or }\frac{|\sigma_3|}{Z_C}, \frac{|\tau_{23}|}{Q}, \frac{|\tau_{13}|}{R}, \frac{|\tau_{12}|}{S}\right\}, \tag{4}$$

where X, Y, Z are tensile or compressive strengths (subscripts 'T' and 'C') along directions 1, 2, 3, respectively; Q, R, S are shear strengths in coordinates 23, 13, 12. Max Stress is straightforward and indicates failure mode. However, predictions can be erroneous due to lack of stress interaction.

A number of quadratic criteria have been developed that account for stress coupling. Azzi and Tsai (1965) proposed an interactive failure criterion, commonly known as Tsai–Hill, based on Hill's modified von Mises criterion for homogenous anisotropic metals (Hill 1948). The coefficient is

$$\begin{aligned} f^{\mathrm{TH}} = {} & \frac{\sigma_1^2}{X_T^2}+\frac{\sigma_2^2}{Y_T^2}+\frac{\sigma_3^2}{Z_T^2}-\sigma_1\sigma_2\left(\frac{1}{X_T^2}+\frac{1}{Y_T^2}-\frac{1}{Z_T^2}\right) \\ & -\sigma_1\sigma_3\left(\frac{1}{X_T^2}-\frac{1}{Y_T^2}+\frac{1}{Z_T^2}\right)-\sigma_2\sigma_3\left(-\frac{1}{X_T^2}+\frac{1}{Y_T^2}+\frac{1}{Z_T^2}\right) \\ & +\frac{\tau_{23}^2}{Q^2}+\frac{\tau_{13}^2}{R^2}+\frac{\tau_{12}^2}{S^2}. \end{aligned} \tag{5}$$

We note exclusive use of tensile strengths in Equation (5), i.e. differences between strengths in tension and compression are unaccounted for. This is a known shortcoming. One can 'artificially' compensate by substituting compressive strengths in directions along which the stress sign is negative. However, in its original form based on von Mises, the fundamental assumption is that tensile and compressive strengths are equal. This is generally not the case for unidirectional FRPs. Another drawback is that no indication of failure mode is given. Nonetheless, Tsai–Hill is universally recognised within the composites community.

Early work by Hashin and Rotem (1973), expanded by Hashin (1980), introduced physical-based criteria that describe heterogeneous failures separately. The Hashin criterion distinguishes

Table 4. Laminate configurations.

TCP	Stacking sequence
A	$[\pm 55]_4$
B	$[\pm 42.5]_4$
C	$[\pm 30]_4$
D	$[(\pm 55)_2/(\pm 30)_2]$

four modes: fibre tension, fibre compression, matrix tension and matrix compression. Coefficients are given below.

Fibre tension ($\sigma_1 > 0$)

$$f^{H1} = \max\left\{\left(\frac{\sigma_1}{X_T}\right)^2 + \frac{(\tau_{12}^2 + \tau_{13}^2)}{R^2}, \frac{\sigma_1}{X_T}\right\}. \quad (6a)$$

Fibre compression ($\sigma_1 < 0$):

$$f^{H2} = \frac{|\sigma_1|}{X_C}. \quad (6b)$$

Matrix tension ($(\sigma_2+\sigma_3) > 0$):

$$f^{H3} = \frac{(\sigma_2 + \sigma_3)^2}{Y_T^2} + \frac{(\tau_{23}^2 - \sigma_2\sigma_3)}{Q^2} + \frac{(\tau_{12}^2 + \tau_{13}^2)}{R^2}. \quad (6c)$$

Matrix compression ($(\sigma_2+\sigma_3) < 0$):

$$f^{H4} = \left(\left(\frac{Y_C}{2Q}\right)^2 - 1\right)\frac{(\sigma_2 + \sigma_3)}{Y_C} + \frac{(\sigma_2 + \sigma_3)^2}{4Q^2} + \frac{(\tau_{23}^2 - \sigma_2\sigma_3)}{Q^2} + \frac{(\tau_{12}^2 + \tau_{13}^2)}{R^2}. \quad (6d)$$

In practice, we consider the largest failure index, i.e.:

$$f^{H} = \max\{f^{H1}, f^{H2}, f^{H3}, f^{H4}\}. \quad (7)$$

3. Results and discussion

3.1. Pure bending

Firstly, we study pure bending prior to bending with temperature change. Properties at 23°C are assumed. We consider the dimensions in Table 1 with different laminates outlined in Table 4. The $[\pm 55]_4$ laminate (TCP A) was chosen as the fibre angle of ±55° is optimal for biaxial pressure and therefore widely employed in piping. It may be prudent to utilise low angles if the TCP is expected to operate under high tension after unspooling, hence $[\pm 42.5]_4$ and $[\pm 30]_4$ sequences (B and C) are investigated. The sequence $[(\pm 55)_2/(\pm 30)_2]$ is studied (D) as it was previously shown to outperform the $[\pm 55]_4$ counterpart under loads illustrative of a deepwater riser application (Hastie et al. 2019b). Under bending, the top ($\theta = 0$ as per Figure 1 coordinates) and bottom ($\theta = \pi$) of the pipe are under axial tension and compression, respectively.

Through-thickness failure coefficients based on von Mises criterion through isotropic liners (r = 76–84 mm, 92–100 mm) and Max Stress through fibre-reinforced laminate (r = 84–92 mm) are shown in Figure 4 for the configurations bent to R = 9 m. The laminate coefficient is consistently higher than the liner coefficient and varies with location. This can be explained with the aid of Table 5, which summarises laminate principal stresses ('mode' is the strength that governs the coefficient, i.e. most utilised). Top and bottom stresses are equal in magnitude with opposite sign, which follows simple bending. TCP A exhibits significantly higher Max Stress coefficient at the top of the pipe compared to the bottom. This is due to the sign of σ_2. Unidirectional layers are weakest under transverse tension that acts to pull fibres apart. At the top, the coefficient is governed by substantial utilisation of transverse tensile strength, whereas at the bottom, it is governed by in-plane shear and is ~37% lower. In TCP B and C with lower fibre angle, the fibre stress, σ_1, is increased but the magnitude of σ_2 is reduced. Consequently, there is no excessive utilisation of transverse strength. Failure is governed by in-plane shear in TCP B and is

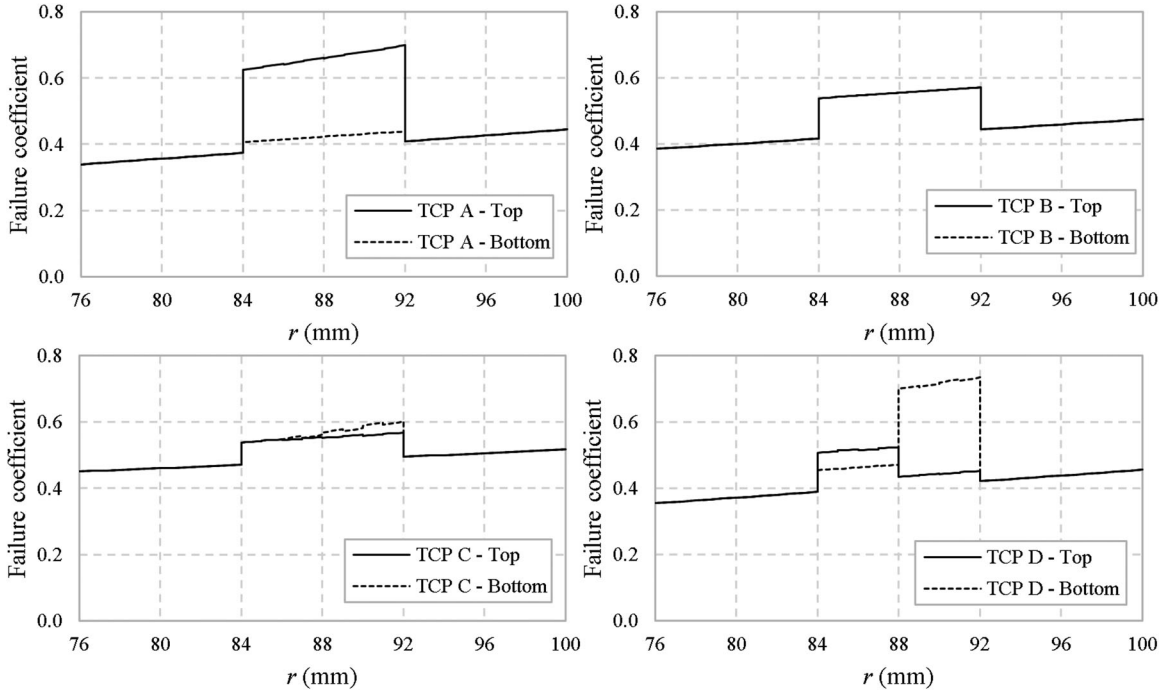

Figure 4. Through-thickness failure coefficients based on von Mises criterion through liners and Max Stress criterion through laminate; pure bending, R = 9m.

Table 5. Laminate stresses; pure bending, $R = 9$m.

TCP	Pipe location	σ_1 (MPa)	σ_2 (MPa)	σ_3 (MPa)	τ_{12} (MPa)	f^{MS}	Mode
A	Top	96.99	55.25	−0.19	81.43	0.70	Y_T
	Bottom	−96.99	−55.25	0.19	−81.43	0.44	S
B	Top	311.68	14.60	−1.66	105.80	0.57	S
	Bottom	−311.68	−14.60	1.66	−105.80	0.57	S
C	Top	723.02	−34.12	−2.88	105.32	0.57	S
	Bottom	−723.02	34.12	2.88	−105.32	0.60	X_C
D	Top	881.54[b]	41.33[a]	−6.07[b]	87.35[a]	0.52[a]	Y_T[a]
	Bottom	−881.54[b]	−41.33[a]	6.07[b]	−87.35[a]	0.73[b]	X_C[b]

[a]±55° layer.
[b]±30° layer.

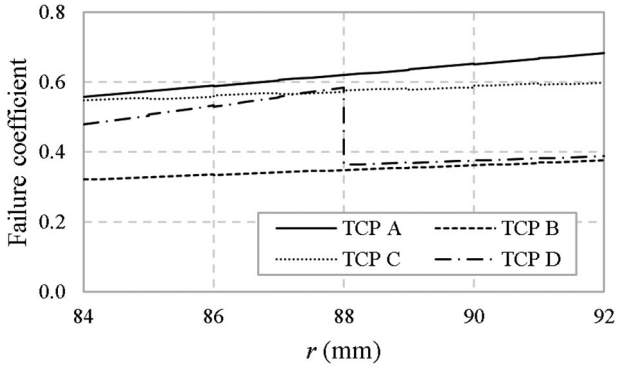

Figure 5. Through-laminate Tsai–Hill coefficients; pure bending, $R = 9$m.

identical at the top and bottom since shear strength is sign-independent. Fibre stresses are largest for TCP C with the lowest fibre angle (±30°). At the bottom of TCP C, the coefficient is governed by fibre compressive strength. Fibre-reinforced laminae are weaker under fibre compression than fibre tension (see Table 2) and the configuration is less optimal than TCP B. Through the multi-angle TCP D laminate, the coefficient is highest in ±55° and ±30° portions at the top and bottom, respectively, and failure modes match the corresponding single-angle configurations. Orientating only a few layers at a low angle results in particularly large fibre compression and is detrimental.

Through-laminate Tsai–Hill and Hashin distributions are shown in Figures 5 and 6 for pure bending. Table 6 summarises the coefficients and Hashin mechanisms (FT, FC, MT, MC are fibre tension, fibre compression, matrix tension, matrix compression). The Tsai–Hill distributions are identical at the pipe top and bottom due to stress symmetry and lack of distinction between tension/compression. All criteria match well at the top of TCP A where transverse and matrix tension are the dominant Max Stress and Hashin modes. At the bottom, the Hashin coefficient is governed by matrix compression and is markedly lower than Max Stress (shear-dominated) and particularly Tsai–Hill, which does not account for sign differences. Fibre tension and compression are the dominant Hashin modes for TCP C with lowest fibre angle at the top and bottom, respectively. We recall the Hashin criterion is equivalent to Max Stress for fibre compression (Equation (6b)) and hence coefficients are equal at the bottom. At the top, the Max Stress shear mode is critical and the Hashin criterion predicts a lower failure coefficient with the inclusion of shear interaction in the fibre tension mode. Overall, the Tsai–Hill and Hashin coefficients are lowest for TCP B, which indicates coefficient is optimal when fibre-reinforced layers are orientated at an 'intermediate' angle and large stresses in transverse and fibre directions are avoided. The Hashin coefficient does not vary significantly with location and is in reasonable agreement with Tsai–Hill. The Max Stress coefficient is also optimal for TCP B, although higher than the alternative criteria. High failure coefficient in the ±30° portion at the bottom of TCP D due to fibre compression is not captured by Tsai–Hill, highlighting that the criterion may dangerously underpredict failure of the multi-angle laminate.

3.2. Bending at temperature

In this section, we investigate the configurations bent to $R = 9$ m at $T = 0$°C and 50°C. The initial temperature of 23°C is assumed. Through-thickness failure coefficients based on von Mises and Max Stress criteria are shown in Figure 7. At 0°C, the von Mises coefficient is higher through both liners at the top of the pipe under tension. On the other hand, the coefficient is higher at the bottom at 50°C and the liners are more susceptible to failure at the elevated temperature (increase of roughly 30% from the maximum coefficient at 0°C for all configurations).

Laminate stresses for 0°C and 50°C cases are summarised in Tables 7 and 8. Temperature change causes deviation from the symmetry expected between stresses at the top/bottom according to

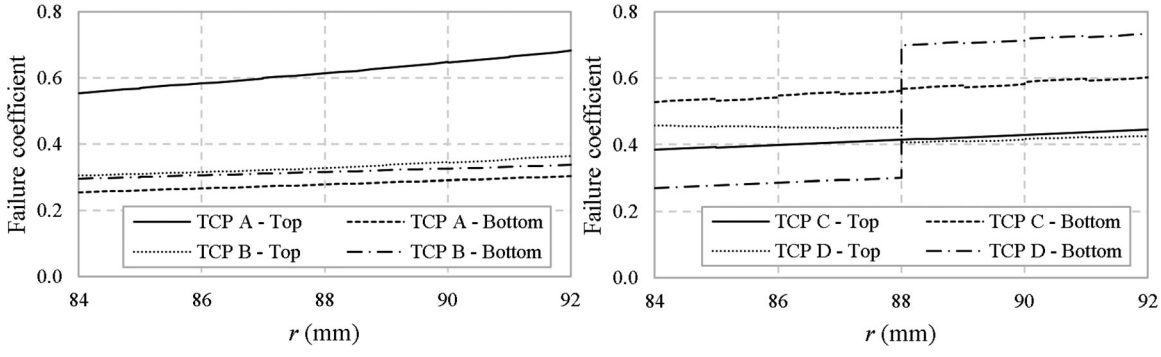

Figure 6. Through-laminate Hashin coefficients; pure bending, $R = 9$m.

Table 6. Laminate Tsai–Hill and Hashin coefficients; pure bending, $R = 9$ m.

TCP	Pipe location	f^{TH}	f^{H} (mode)
A	Top	0.68	0.68 (MT)
	Bottom		0.30 (MC)
B	Top	0.38	0.36 (MT)
	Bottom		0.34 (MC)
C	Top	0.60	0.45 (FT)
	Bottom		0.60 (FC)
D	Top	0.58[a]	0.46[a] (MT)
	Bottom		0.73[b] (FC)

[a]±55° layer.
[b]±30° layer.

simple bending. At 0°C, the magnitude of $-\sigma_1$ at the bottom of the pipe is larger than σ_1 at the top. The difference is greatest for TCP A (~79%). Conversely, $|\sigma_1|$ at the bottom is smaller than σ_1 at the top at 50°C (~54% smaller in TCP A). Max Stress coefficient for TCP A is governed by transverse tension at the top and is virtually identical at 0°C and 50°C. In other words, there is effectively a balance between ratios of higher stress and strength at 0°C and lower stress and strength at 50°C. However, at the bottom, the mode is in-plane shear and the coefficient is lower at elevated temperature. Coefficient for TCP B is governed by in-plane shear and does not vary significantly with location or temperature. This may be desirable from a design point-of-view. Modes for TCP C at 0°C follow pure

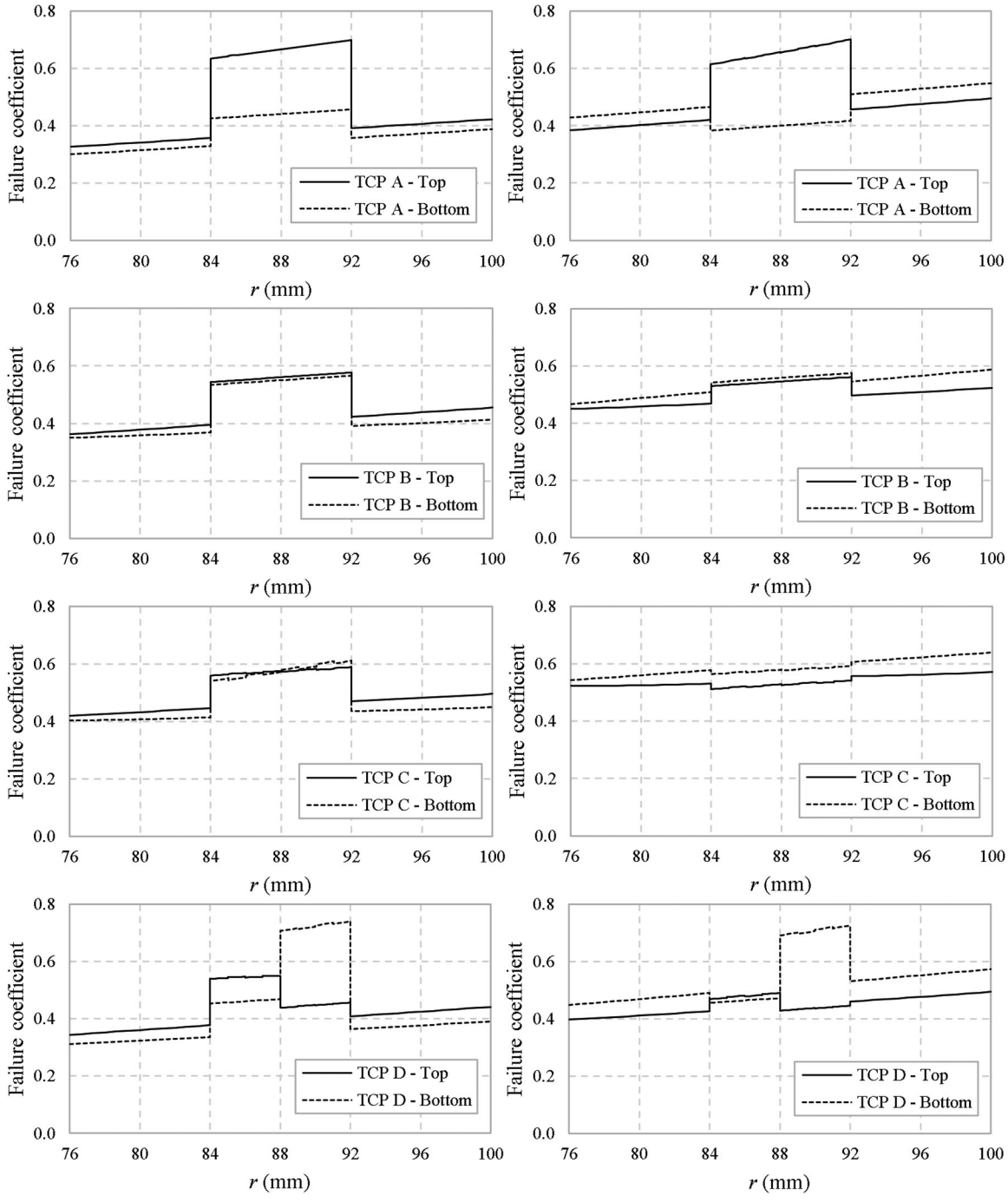

Figure 7. Through-thickness failure coefficients based on von Mises criterion through liners and Max Stress criterion through laminate; $R = 9$m at $T = 0$°C (left) and 50°C (right).

Table 7. Laminate stresses; $R = 9$ m, $T = 0$°C. The percentages show the increase/decrease at the pipe bottom with respect to the top.

TCP	Pipe location	σ_1 (MPa)	σ_2 (MPa)	σ_3 (MPa)	τ_{12} (MPa)	f^{MS}	Mode
A	Top	74.26	58.02	0.66	82.96	0.70	Y_T
	Bottom	−132.84	−56.40	0.89	−89.16	0.46	S
		(+78.87%)	(−2.79%)	(+35.52%)	(+7.47%)	(−34.29%)	
B	Top	294.35	17.91	−1.00	112.63	0.58	S
	Bottom	−356.25	−13.42	2.40	−110.47	0.57	S
		(+21.03%)	(−25.10%)	(+140.95%)	(−1.92%)	(−1.72%)	
C	Top	722.58	−34.20	−2.42	114.82	0.59	S
	Bottom	−768.84	33.66	3.42	−106.77	0.61	X_C
		(+6.40%)	(−1.57%)	(+41.31%)	(−7.01%)	(+3.39%)	
D	Top	876.92[b]	45.67[a]	−6.42[b]	92.79[a]	0.55[a]	Y_T[a]
	Bottom	−932.26[b]	−40.47[a]	5.85[b]	−91.57[a]	0.74[b]	X_C[b]
		(+6.31%)	(−11.39%)	(−8.86%)	(−1.31%)	(+34.55%)	

[a]±55° layer.
[b]±30° layer.

Table 8. Laminate stresses; $R = 9$ m, $T = 50$°C. The percentages show the increase/decrease at the pipe bottom with respect to the top.

TCP	Pipe location	σ_1 (MPa)	σ_2 (MPa)	σ_3 (MPa)	τ_{12} (MPa)	f^{MS}	Mode
A	Top	122.31	52.23	−0.94	79.42	0.70	Y_T
	Bottom	−56.52	−53.67	−0.83	−72.60	0.42	S
		(−53.79%)	(+2.75%)	(−11.48%)	(−8.59%)	(−40.00%)	
B	Top	330.98	10.99	−2.43	97.81	0.56	S
	Bottom	−261.08	−15.80	0.82	−100.20	0.58	S
		(−21.12%)	(+43.67%)	(−66.08%)	(+2.45%)	(+3.57%)	
C	Top	722.84	−33.63	−3.42	94.40	0.54	S
	Bottom	−671.36	34.70	2.29	−103.14	0.59	S
		(−7.12%)	(+3.18%)	(−32.99%)	(+9.27%)	(+9.26%)	
D	Top	885.72[b]	36.50[a]	−5.68[b]	80.99[a]	0.49[a]	Y_T[a]
	Bottom	−823.40[b]	−42.10[a]	6.32[b]	−82.31[a]	0.73[b]	X_C[b]
		(−7.04%)	(+15.34%)	(+11.22%)	(+1.62%)	(+48.98%)	

[a]±55° layer.
[b]±30° layer.

bending, i.e. transverse tension at the top and fibre compression at the bottom. Compressive fibre stress is lower at 50°C and the mode for both locations is in-plane shear. As per pure bending, there is very high compressive stress along ±30° fibres in TCP D. This stress and corresponding failure coefficient are higher than the pure bending case at 0°C and lower at 50°C.

The Tsai–Hill and Hashin distributions are shown in Figures 8 and 9 and coefficients/modes are summarised in Table 9 for the case of $R = 9$ m at temperature. The Tsai–Hill coefficient for TCP A does not vary with location and is slightly higher at 50°C than at 0°C. The coefficient through TCP B and C laminates is higher at the top of the pipe at 0°C and at the bottom of the pipe at 50°

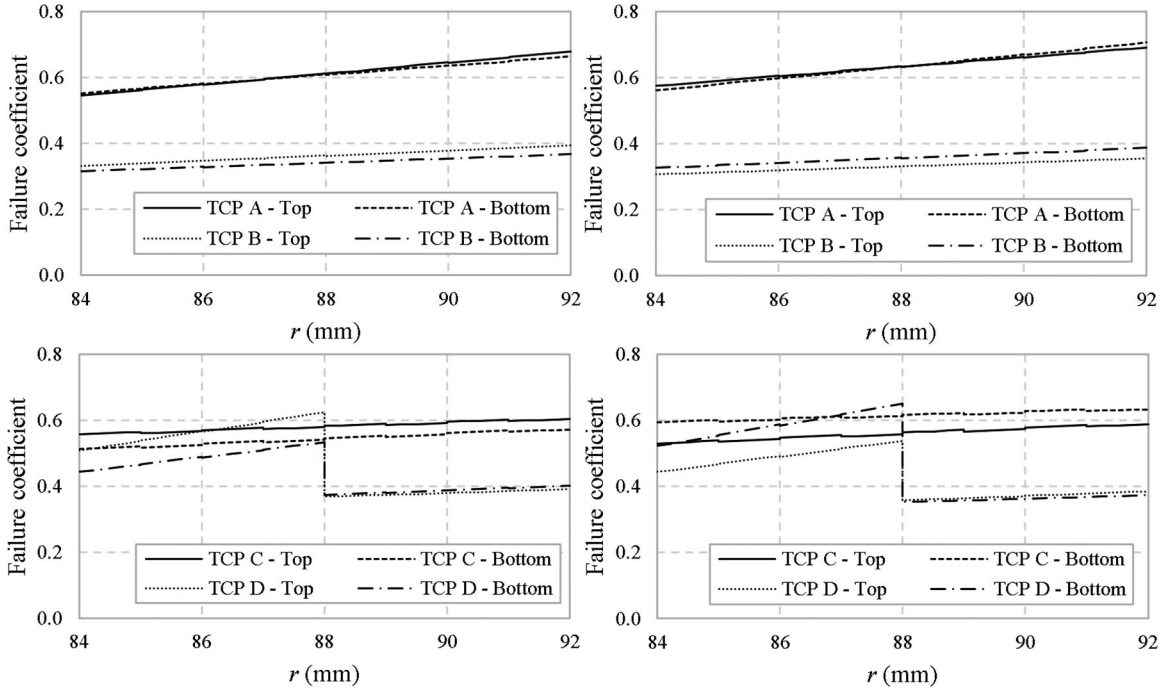

Figure 8. Through-laminate Tsai–Hill coefficients; $R = 9$m at $T = 0$°C (left) and 50°C (right).

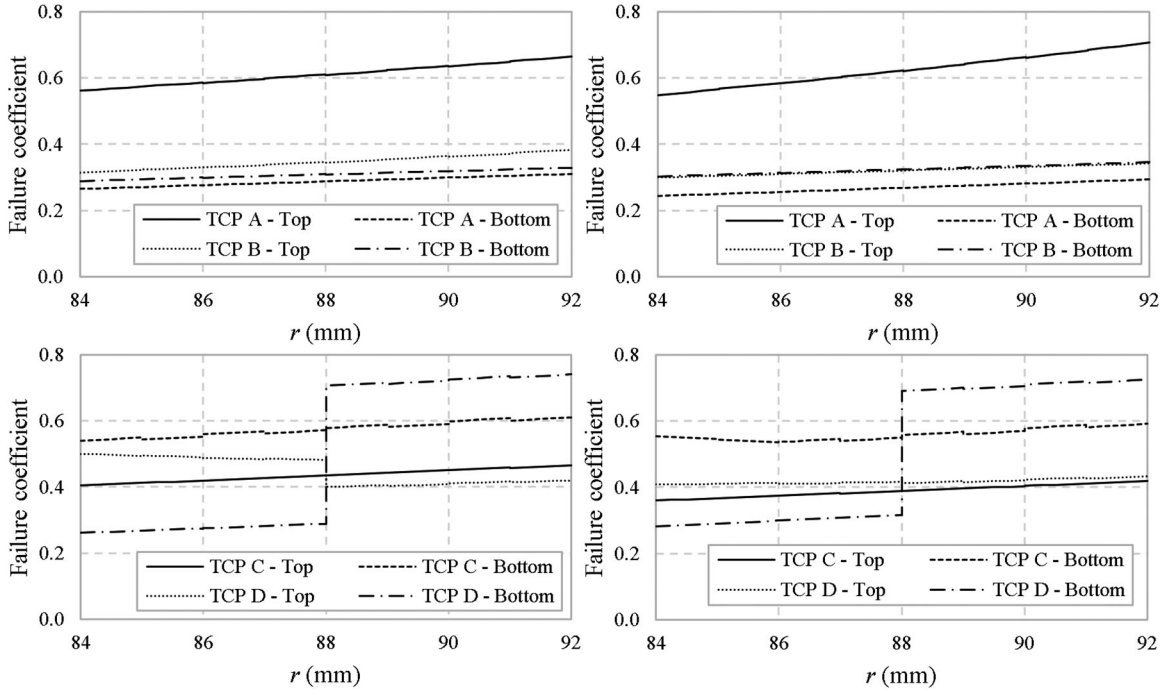

Figure 9. Through-laminate Hashin coefficients; $R = 9$m at $T = 0$°C (left) and 50°C (right).

C. The same is true for the ±55° innermost layers of TCP D, while coefficient through the ±30° portion does not vary with location. The Tsai–Hill and Hashin results match closely for TCP A at the top of the pipe where the failure coefficient is high and the dominant Hashin mode is matrix tension, as was the case for pure bending. Again, at the bottom, the Hashin mode is matrix compression and failure coefficient is significantly lower than the top, particularly at 50°C (~59% reduction). The Hashin coefficient through TCP B does not vary significantly with location or temperature and is in reasonable agreement with Tsai–Hill. Overall, TCP B ($[\pm 42.5]_4$) exhibits the lowest failure coefficients at both temperatures. As was observed for pure bending, the Hashin coefficient through TCP C with the lowest fibre angle is governed by fibre tension at the top of the pipe and fibre compression at the bottom and noticeably higher failure coefficient is observed at the bottom at both temperatures. Similarly, the Hashin coefficient is high through the ±30° layers at the bottom of TCP D.

3.3. Comparison of practical bending radii

We now consider practical implications of fibre angle optimisation on spooling. Liner von Mises and laminate Hashin coefficients vs. bending radius are shown in Figures 10 and 11 for TCP A and B over the range $R = 5$–10 m at $T = 0$°C and 50°C. Liner responses are very similar for both configurations. The yielding of the outer liner is expected to occur at roughly $R = 5$ m at 50°C. On the other hand, liner yielding is not expected under $R = 5$ m at 0° with maximum von Mises coefficients of 0.74 for TCP A and 0.80 for TCP B.

It is clear from the Hashin results that TCP B ($[\pm 42.5]_4$) can be spooled to a tighter radius than TCP A ('classic' $[\pm 55]_4$). The TCP A laminate is predicted to fail at the top of the pipe at approximately $R = 7.5$ m at both temperatures. We see that for $R = 7.5$ m, the coefficient at the bottom is only 0.44 at 0°C and 0.42 at 50°C, which emphasises the disparity due to off-axis tensioning of ±55° layers. The bending of TCP A to $R = 10$ m at 50°C results in a maximum Hashin coefficient of 0.57, i.e. corresponding to the reciprocal safety factor of 1.75. A higher factor of 1.85 is exhibited at 0°C. Meanwhile, failure of the TCP B laminate occurs when $R = 5.5$ m at 0°C and approximately 5.25 m at 50°C. TCP B can be bent to $R = 7.5$ m with maximum coefficients of 0.55 at 0°C and 0.49 at 50°C, giving safety factors of 1.82 and 2.04. In other words, the TCP B laminate is slightly over and under 50% utilised when bent to the failure radius of TCP A at 0°C and 50°C, respectively. At the higher temperature, liner utilisation (almost 70% for outer liner) would exceed that of the laminate. This is generally favourable when we consider the ability to perform field repairs and greater industry acceptance of isotropic material predictions.

Table 9. Laminate Tsai–Hill and Hashin coefficients; $R = 9$ m, $T = 0$°C and 50°C.

		$T = 0$°C		$T = 50$°C	
TCP	Pipe location	f^{TH}	f^{H} (mode)	f^{TH}	f^{H} (mode)
A	Top	0.68	0.67 (MT)	0.69	0.71 (MT)
	Bottom	0.67	0.31 (MC)	0.71	0.29 (MC)
B	Top	0.39	0.38 (MT)	0.36	0.34 (MT)
	Bottom	0.37	0.33 (MC)	0.39	0.35 (MC)
C	Top	0.60	0.47 (FT)	0.59	0.42 (FT)
	Bottom	0.57	0.61 (FC)	0.63	0.59 (FC)
D	Top	0.62[a]	0.50[a] (MT)	0.54[a]	0.43[b] (FT)
	Bottom	0.53[a]	0.74[b] (FC)	0.65[a]	0.73[b] (FC)

[a]±55° layer.
[b]±30° layer

3.4. Discussion

A fibre angle of ±55° is optimal for biaxial pressure and widely used for laminated tubulars. However, TCP A studied here with $[\pm 55]_4$ sequence exhibited a high failure coefficient under bending caused by transverse tensile stress at the top of the pipe. Conversely, layers stacked in the arrangement $[\pm 30]_4$ (TCP C) are susceptible to failing at the bottom under fibre compression. This stress is particularly high at reduced temperature. Moreover, low angles may be unsuitable if the intention beyond spooling is to operate the TCP in

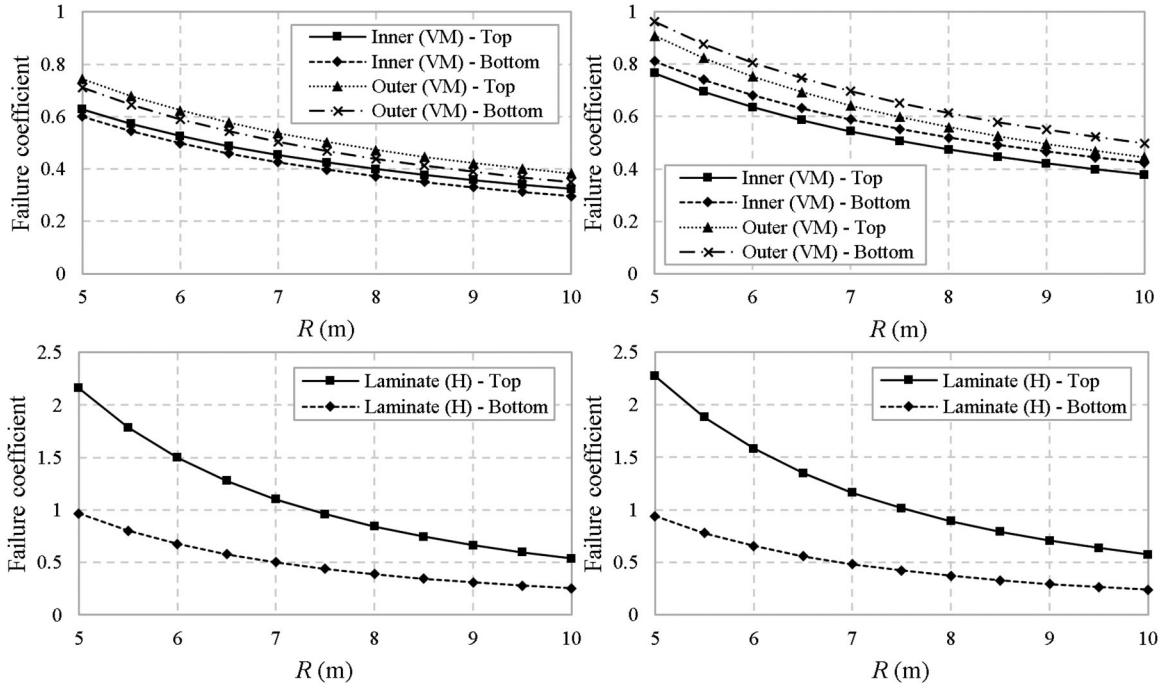

Figure 10. Liner von Mises (VM) and laminate Hashin (H) coefficient vs. *R*; TCP A at $T = 0°C$ (left) and 50°C (right).

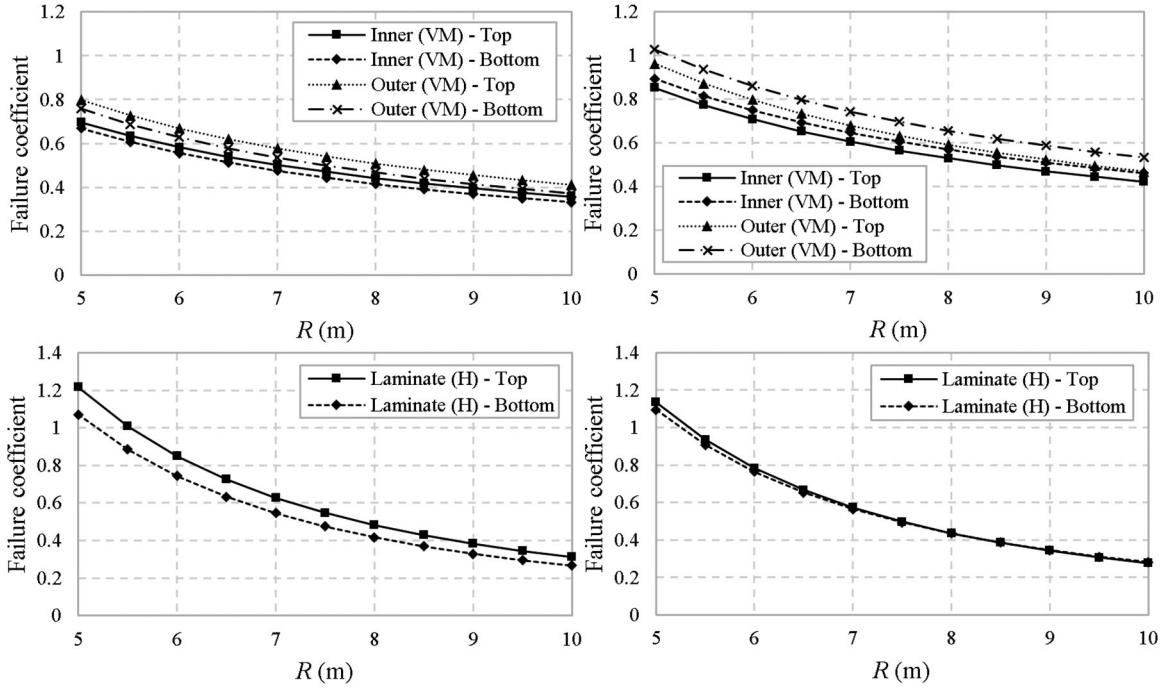

Figure 11. Liner von Mises (VM) and laminate Hashin (H) coefficient vs. *R*; TCP B at $T = 0°C$ (left) and 50°C (right).

deepwater under high pressures where circumferential reinforcement is imperative.

Of the configurations studied, the optimal failure coefficient is achieved using the intermediate fibre angle of ±42.5° where in-plane shear is dominant and excessive transverse tensile and fibre compressive loads are avoided. In practical terms, TCP B can be spooled to tighter radius than its counterparts. Furthermore, failure predictions for the TCP B laminate did not vary significantly with location or temperature. It is desirable for performance to remain as constant as possible for both cold and hot environments. This may allow the TCP to be stored and deployed in a wider range of thermal settings while remaining within desired safety margins. It should be noted that isotropic liners exhibit asymmetric von Mises coefficient at the top and bottom under bending with temperature change and are more susceptible to yielding at raised temperature. Higher utilisation of isotropic layers relative to composite layers is favourable in terms of repairability and greater industry confidence in isotropic predictions. Given that the liner function is wear resistance and fluid-tightness, it could be suggested that yielding does not necessarily constitute loss of function. Alternative failure rules could be investigated.

The optimisation of fibre orientation for spooling will have implications on the performance of the TCP when in subsequent operation and subjected to different loads. Thus, both spooling and operating stages must be carefully considered in conjunction during the design phase. For the same dimensions, the $[(\pm55)_2/(\pm30)_2]$ arrangement was previously shown to be effective when operating under combined pressures, thermal gradient and high tension illustrative of a deepwater riser application (Hastie et al. 2019b). Based on results of the current paper, tailoring the laminate for deepwater operation by orientating a portion of layers at a low angle would have a detrimental effect on spooling capacity due to high utilisation of fibre compressive strength. This would ultimately necessitate larger spools.

In this work, Max Stress, Tsai–Hill and Hashin criteria were employed to evaluate macroscopic failure. These have been used over many years with varying success. Rodriguez and Ochoa (2004) notably employed the Hashin criterion for plane stress in predicting progressive damage of FRP tubes under bending with thermal residual stresses. More recently, Huang et al. (2020) predicted failure of filament-wound pipes under bending accurately by progressive damage modelling with 2D Hashin modes. TCP is high cost and an experimental programme to assess the accuracy of criteria for the 3D case and bending/thermal combination was outwith this project scope. Nevertheless, the comparisons here provide useful insight for design of TCP in line with industry guidelines, which dictate Max Stress is satisfied and other criteria are permissible provided they are 'equal or conservative' (DNV GL 2018). Renowned Tsai–Hill and Hashin criteria will always likely enter discussions on failure. Max Stress, Tsai–Hill and Hashin agreed on $[\pm42.5]_4$ being the superior configuration here. The criteria were in close agreement at the top of the pipe under axial tension when transverse/matrix tension was dominant. Tsai–Hill failed to capture significant differences at opposing locations, which is shown to be particularly significant in a multi-angle laminate with portion of low angle layers. With respect to Hashin, Max Stress over-predicted failure when in-plane shear was dominant and stress interaction was unaccounted for. Comprehensive experimental work to assess the accuracy of criteria for the combined loading condition can be conducted in future. This can be undertaken with a view to informing standards and improving utilisation. In an industrial scenario, the present modelling approach can provide a solid foundation for early design prior to qualification testing.

4. Conclusions

A 3D FE model was developed to analyse stresses in a section of TCP under combined bending and uniform temperature change illustrative of spooling in different environments. Material temperature-dependency was considered.

The following important findings were made:

- Temperature change causes deviation from the symmetry expected between stresses at the top and bottom of the pipe in simple bending. As such, stress-based failure coefficients depend on circumferential location.
- TCP can be optimised for spooling by orientating unidirectional layers at an intermediate fibre angle that avoids excessive loading along transverse and fibre directions.
- The $[\pm42.5]_4$ configuration exhibited the superior spooling capacity of those studied here. Utilisation of the $[\pm42.5]_4$ laminate was 55% and 49% when bent to the failure radius (roughly $R = 7.5$ m) of the $[\pm55]_4$ counterpart at 0°C and 50°C, respectively, according to the Hashin criterion.
- Max Stress, Tsai–Hill and Hashin criteria were in closest agreement at the top of the pipe under tension when transverse/matrix tension modes were dominant. Coefficients differed more significantly at the bottom, which exhibited large compressive or in-plane shear stresses. Tsai–Hill may critically underpredict failure at the bottom of a multi-angle pipe with few low angle layers under high fibre compression.
- Tailoring TCP for spooling can have a negative effect on operating performance and vice versa. A laminate configuration of $[(\pm55)_2/(\pm30)_2]$ was shown in earlier work to be effective under axisymmetric loads illustrative of deepwater operation but in this study was found to exhibit high failure coefficient in low angle layers under bending. Spooling and operating stages must be considered in conjunction during the design phase.

The presented results illustrate response of a carbon/PEEK TCP and manufacturers may use an identical approach to quantify the performance of alternative configurations and materials (e.g. glass- or hybrid-reinforced PA, PVDF etc.). In real-world design, material properties should be actively determined by testing rather than relying on properties listed elsewhere, as was the case here in order to show representative results.

Disclosure statement

No potential conflict of interest was reported by the author(s).

ORCID

James C. Hastie http://orcid.org/0000-0002-6408-6005
Igor A. Guz http://orcid.org/0000-0003-2683-7530
Maria Kashtalyan http://orcid.org/0000-0003-1950-5677

References

Akçay İH, Kaynak İ. 2005. Analysis of multilayered composite cylinders under thermal loading. J Reinf Plast Compos. 24(11):1169–1179.
Almeida Jr. JHS, Tonatto MLP, Faria H, Marques AT, Amico SC. 2014. Effect of environmental conditioning on burst pressure of carbon/epoxy filament wound composite pipes. 16th European Conference on Composite Materials; Seville; Spain, 22–26 June.
Ashraf MA, Morozov EV, Shankar K. 2014. Flexure analysis of spoolable reinforced thermoplastic pipes for offshore oil and gas applications. J Reinf Plast Compos. 33(6):533–542.
Azzi VD, Tsai SW. 1965. Anisotropic strength of composites. Exp Mech. 5:283–288.
Bai Y, Ruan W, Cheng P, Yu B, Xu W. 2014. Buckling of reinforced thermoplastic pipe (RTP) under combined bending and tension. Ships Offsh Struct. 9 (5):525–539.
Bai Y, Yu B, Cheng P, Wang N, Ruan W, Tang J, Babapour A. 2015a. Bending behavior of reinforced thermoplastic pipe. J Offshore Mech Arct Eng. 137 (2):021701.
Bai Y, Yuan S, Tang J, Qiao H, Cheng P, Cao Y, Wang N. 2015b. Behaviour of reinforced thermoplastic pipe under combined bending and external pressure. Ships Offsh Struct. 10(5):575–586.
Bakaiyan H, Hosseini H, Ameri E. 2009. Analysis of multi-layered filament-wound composite pipes under combined internal pressure and thermomechanical loading with thermal variations. Compos Struct. 88(4):532–541.
Cao Y, Yu X, Liu Z, Bai Y, Gong X. 2017. On critical design parameters of reinforced thermoplastic pipes associated with the pipe-lay installation. Ships Offsh Struct. 12(Suppl. 1):S134–S143.
Coquill SL, Adams DF. 1989. Mechanical properties of several neat polymer matrix materials and unidirectional carbon fiber-reinforced composites. NASA CR-181805.
Cox K, Menshykova M, Menshykov O, Guz I. 2019. Analysis of flexible composites for coiled tubing applications. Compos Struct. 225:111118.
Cytec. 2012. APC-2 PEEK thermoplastic polymer technical data sheet.
DNV GL. 2018. Standard DNVGL-ST-F119 thermoplastic composite pipes.
Geuchy Ahmad MI, Hoa SV. 2016. Flexural stiffness of thick walled composite tubes. Compos Struct. 149:125–133.

Grove SM. 1988. Thermal modelling of tape laying with continuous carbon fibre-reinforced thermoplastic. Composites. 19(5):367–375.
Guz IA, Menshykova M, Paik JK. 2017. Thick-walled composite tubes for offshore applications: an example of stress and failure analysis for filament-wound multi-layered pipes. Ships Offsh Struct. 12(3):304–322.
Hashin Z. 1980. Failure criteria for unidirectional fiber composites. J Appl Mech. 47(2):329–334.
Hashin Z, Rotem A. 1973. A fatigue failure criterion for fiber reinforced materials. J Compos Mater. 7(4):448–464.
Hastie JC, Guz IA, Kashtalyan M. 2019a. Effects of thermal gradient on failure of a thermoplastic composite pipe (TCP) riser leg. Int J Press Vessels Pip. 172:90–99.
Hastie JC, Guz IA, Kashtalyan M. 2020. Structural integrity of deepwater composite pipes under combined thermal and mechanical loading. Procedia Struct Integr. 28:850–863.
Hastie JC, Kashtalyan M, Guz IA. 2019b. Failure analysis of thermoplastic composite pipe (TCP) under combined pressure, tension and thermal gradient for an offshore riser application. Int J Press Vessels Pip. 178:103998.
Hastie JC, Kashtalyan M, Guz IA. 2021. Analysis of filament-wound sandwich pipe under combined internal pressure and thermal load considering restrained and closed ends. Int J Press Vessels Pip. 191:104350.
Hill R. 1948. A theory of the yielding and plastic flow of anisotropic metals. Proc R Soc Lond A Math Phys Sci. 193(1033):281–297.
Huang Z, Qian X, Su Z, Pham DC, Sridhar N. 2020. Experimental investigation and damage simulation of large-scaled filament wound composite pipes. Composites Part B: Eng. 184:107639.
Jolicoeur C, Cardou A. 1994. Analytical solution for bending of coaxial orthotropic cylinders. J Eng Mech. 120(12):2556–2574.
Jones DP, Leach DC, Moore DR. 1985. Mechanical properties of poly(ether-ether-ketone) for engineering applications. Polymer. 26(9):1385–1393.
Ju GT, Kyriakides S. 1992. Bifurcation and localization instabilities in cylindrical shells under bending—II. predictions. Int J Solids Struct. 29(9):1143–1171.
Kyriakides S, Ju GT. 1992. Bifurcation and localization instabilities in cylindrical shells under bending—I. experiments. Int J Solids Struct. 29(9):1117–1142.
Meng M, Le HR, Rizvi MJ, Grove SM. 2015. The effects of unequal compressive/tensile moduli of composites. Compos Struct. 126:207–215.
Menshykova M, Guz IA. 2014. Stress analysis of layered thick-walled composite pipes subjected to bending loading. Int J Mech Sci. 88:289–299.
Moshir SK, Hoa SV, Shadmehri F, Rosca D, Ahmed A. 2020. Mechanical behavior of thick composite tubes under four-point bending. Compos Struct. 242:112097.
Natsuki T, Takayanagi H, Tsuda H, Kemmochi K. 2003. Prediction of bending strength for filament-wound composite pipes. J Reinf Plast Compos. 22(8):695–710.
Ramey J, Palazotto A. 1989. A study of graphite/PEEK under high temperatures. In: G.M. Newaz, editor. Advances in thermoplastic matrix composite materials. West Conshohocken, PA: ASTM; p. 91–112.
Rodriguez DE, Ochoa OO. 2004. Flexural response of spoolable composite tubulars: an integrated experimental and computational assessment. Compos Sci Technol. 64(13–14):2075–2088.
Rule DL, Sparks LL. 1990. Thermal conductivity of alumina fiber/epoxy and alumina fiber/PEEK from 4.2 to 310 K. In: C.J. Cremers, H.A. Fine, editors. Thermal conductivity 21. New York, NY: Plenum; p. 671–683.
Shadmehri F, Derisi B, Hoa SV. 2011. On bending stiffness of composite tubes. Compos Struct. 93(9):2173–2179.
Smits A, Neto TB, de Boer H. 2018. Thermoplastic composite riser development for ultradeep water. Offshore Technology conference; Houston, TX, USA, 30 April–3 May. OTC-29061-MS.
Sun CT, Rui Y. 1989. Orthotropic elasto-plastic behavior of AS4/APC-2 thermoplastic composite in compression. NASA CML. 89-2.
van Onna M, de Kanter J, Steuten B. 2012. Advancements in thermoplastic composite riser development. 31st International Conference on Ocean, Offshore and Artic Engineering; Rio de Janeiro, Brazil, 1–6 July. ASME, pp. 335–343.
Xia M, Kemmochi K, Takayanagi H. 2001. Analysis of filament-wound fiber-reinforced sandwich pipe under combined internal pressure and thermo-mechanical loading. Compos Struct. 51(3):273–283.
Xia M, Takayanagi H, Kemmochi K. 2002. Bending behavior of filament-wound fiber-reinforced sandwich pipes. Compos Struct. 56(2):201–210.
Yousefpour A, Nejhad MNG. 2004. Design, analysis, manufacture, and test of APC-2/AS4 thermoplastic composite pressure vessels for deep water marine applications. J Compos Mater. 38(19):1701–1732.
Yu K, Morozov EV, Ashraf MA, Shankar K. 2015. Analysis of flexural behaviour of reinforced thermoplastic pipes considering material nonlinearity. Compos Struct. 119:385–393.
Zhang Q, Wang ZW, Tang CY, Hu DP, Liu PQ, Xia LZ. 2012. Analytical solution of the thermo-mechanical stresses in a multilayered composite pressure vessel considering the influence of the closed ends. Int J Press Vessels Pip. 98:102–110.